frontiers | Frontiers in Earth Science

TYPE Original Research
PUBLISHED 09 April 2025
DOI 10.3389/feart.2025.1572526

OPEN ACCESS

EDITED BY
Hao Shi,
Anhui University of Science and Technology, China

REVIEWED BY
Junqing Guo,
Taiyuan University of Technology, China
Rui Wu,
Jiangxi University of Science and Technology, China

*CORRESPONDENCE
Lei Sun,
tb23020029a41@cumt.edu.cn
Xiaowu Zhang,
xwzh667@cumt.edu.cn
Zhijun Xu,
tb20020034b0@cumt.edu.cn

RECEIVED 07 February 2025
ACCEPTED 25 March 2025
PUBLISHED 09 April 2025

CITATION
Cao Y, Sun L, Zhang X, Xu Z, Tai L, Zheng Y and Wu P (2025) Study on mechanical properties and acoustic emission characteristics of concrete-high water composites under uniaxial compression. *Front. Earth Sci.* 13:1572526. doi: 10.3389/feart.2025.1572526

Study on mechanical properties and acoustic emission characteristics of concrete-high water composites under uniaxial compression

Yue Cao[1], Lei Sun[1]*, Xiaowu Zhang[1]*, Zhijun Xu[1]*, Lianhai Tai[1], Yadong Zheng[1] and Peng Wu[2]

[1]School of Mining Engineering, China University of Mining and Technology, Xuzhou, China, [2]School of Physics and New Energy, Xuzhou University of Technology, Xuzhou, China

Under complex stress, a rigid filling body can easily cause the shear failure of the gob-side entry retaining (GSER) roof, and a flexible filling body can easily cause serious deformation of the roadway side. The combined filling body with a soft upper and rigid lower can respond to the needs of support strength and deformation of GSER. In this paper, the uniaxial compression test and acoustic emission (AE) characteristic test of concrete-high water composite (CHWC) specimens with different height ratios (Height ratios = High water layer height/CHWC specimens height) were performed to explore the influence of height ratio on the strength and deformation of CHWC specimens. The test results show that when the height ratio is 10% and 20%, the stress-strain characteristic curve of the CHWC specimens has secondary compaction, elastic, and plastic stages. The peak compressive strength of CHWC specimens is negatively correlated with the height of the high water layer and positively correlated with the height of the concrete layer. The peak strain of the CHWC specimens increases first and then declines with the increase of the height ratio. When the height ratio is ≤20%, the concrete layer of the CHWC specimens plays a major role in the bearing capacity. The peak strain of the CHWC specimens is about 224.4% and 348% of the uttermost strain of the pure concrete specimen (the same composition ratio of concrete). When the height ratio is ≥30%, the overall bearing structure of the CHWC specimens gradually fails after the failure and instability of the high water layer, and the concrete stratification fails to give full play to the bearing role. The research results can provide a reference for applying combined filling technology in GSER.

KEYWORDS

uniaxial loading, concrete-high water composite specimen, mechanical properties, failure mode, acoustic emission

1 Introduction

Coal is the primary energy source in China, underground mining accounts for nearly 80%, yet the coal recovery rate remains between 21% and 52% (Wu et al., 2019). GSER can realize coal pillarless mining by constructing a roadside filling body, which is widely

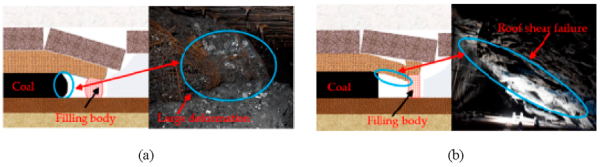

FIGURE 1
Failure form of gob-side entry retaining. **(a)** Concrete. **(b)** High water materials.

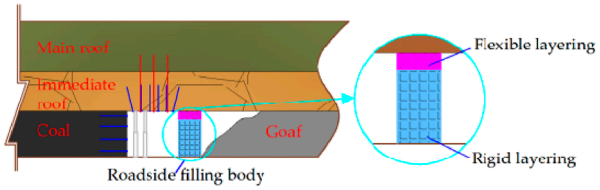

FIGURE 2
Combined filling schematic.

used in underground mining (Tian et al., 2020; Li et al., 2023). As the main structure of supporting the roof and isolating goaf, the stability of the filling body beside the roadway is crucial for the success of GSER. Currently, the commonly used methods for GSER roadside filling bodies adjacent to the flexible formwork concrete (Zhu et al., 2024; Cao X. et al., 2024; Chen et al., 2023) and high-water materials (Zhang et al., 2023; Li and Liu, 2018). However, the lack of flexibility in the concrete filling body can lead to shear failure of the roof (Kong et al., 2021), as illustrated in Figure 1a. Conversely, high-water material filling bodies exhibit considerable deformation under high stress and cannot provide high-strength support (Cheng et al., 2020), as shown in Figure 1b. The combined filling of GSER has been proposed to address these issues, as depicted in Figure 2. Furthermore, cemented coal gangue backfill materials are gradually being applied in GSER (Wu et al., 2022; Wu et al., 2025a), yet the conflict between the material's resistance to deformation and its compressive performance remains challenging to reconcile (Wu et al., 2024; Wu et al., 2025b). The upper and lower parts of the filling body adjacent to the roadway are cast from flexible and rigid materials, respectively, forming a combined structure with a soft upper layer and a rigid lower layer. Successful implementation hinges on the optimal design of these layers to satisfy deformation and strength criteria. Therefore, the study of mechanical properties and AE characteristics of CHWC under uniaxial compression is crucial for engineering applications.

Current research on the mechanical properties of composite materials emphasizes coal-rock composites (Karacan, 2015; Wang et al., 2016), rock-coal-rock composites (He et al., 2021), and rock-filling composites (Zhang et al., 2022). Studies investigate mechanical behavior by varying layer proportions (Lei et al., 2023), material strengths (Cao et al., 2019; Bingchao et al., 2023), quantities (Liu et al., 2024), interface angles (Pan et al., 2021), loading methods (Yu et al., 2021; Wu et al., 2020), and external environments (Liu et al., 2024). Zhao Z. et al. (2015) found that the peak compressive strength and elastic modulus of coal-rock composites are intermediate between coal and rock. Ma et al. (2021) noted a decrease in mechanical properties with increased coal body height, while the coal body's strength significantly influences composite strength (Yin et al., 2019). Increased rock strength can shift failure modes towards tensile failure (He et al., 2021). Liu et al. (2024) tested mudstone-clay composites under varying conditions, focusing on moisture effects on coal-rock and rock-coal-rock composites. Guo et al. (2011) examined interface angles' impact on mechanical behavior and failure modes. Several studies have also explored loading method effects on coal-rock composites (Lu et al., 2020; Ma et al., 2022; Wang et al., 2024), yet insufficient attention has been given to filling materials. Zhang et al. (2022) conducted uniaxial compression tests on water-sand filling and red sandstone, revealing that filling body strength influences overall load-bearing capacity. Zhao et al. (2022) supported this finding. Tan et al. (2018) investigated loading method impacts on rock-filling composites. Selçuk and Aşma (2019) studied interface responses in rock-concrete composites, finding that increasing interface angles (0°–45°) transitions failure modes from axial tensile to shear failure. Chen et al. (2020) evaluated compressive performance under static and dynamic loads, showing that fiber-reinforced concrete enhances mechanical properties. Koupouli et al. (2016) examined shear issues between cemented paste backfill and rock interfaces, finding the former's shear strength superior. However, research on rigid-flexible composite materials, particularly the influence of height ratios on mechanical performance, remains limited.

Despite the abundant research findings on the mechanical behavior of rock composite materials and rock-filling composite materials, reports on the mechanical properties and AE characteristics of CHWC materials are relatively scarce. The roadside filling body of GSER needs to have stress adaptability and deformation adaptability, it has the ability of superior strength bearing while providing deformation space. At present, it is difficult for a single structural filling body under complex stress to have both of the above properties (Figure 1), which leads to intense deformation of the roadway and difficulties in subsequent support. To study the deformation and failure characteristics of CHWC specimens, the paper conducts a series of uniaxial compression and AE experiments on CHWC specimens with varying height ratios. The focus is placed on investigating the stress-strain behavior, failure modes, and AE characteristics of the CHWC specimens, as well as exploring the influence of height ratios on their mechanical behavior.

2 Experimental materials and methods

2.1 Experimental materials and preparation

The materials for the upper and lower layers of the composite specimens were chosen as high-water materials with a water-to-cement ratio of 1.2:1 (Jianbiao et al., 2022) and C40 concrete (Chen et al., 2023). The composition and ratio of concrete and high water materials are shown in Table 1. A material, A material additive and water are stirred separately, B material, B material additive and water are stirred separately, and then the slurry is mixed (high water materials). Standard cubic concrete specimens

TABLE 1 Composition and ratio of concrete and high water materials. The composition ratio of concrete and foamed cement: ratio to the weight of 42.5 ordinary Portland cement.

Concrete composition and ratio	42.5 ordinary portland cement	Sand (fineness modulus of 2.6 ~ 3.0)		5 ~ 20 mm continuous graded crushed stone		Water
	1	0.875		0.9375		0.375
High water materials composition and ratio	A material	A material additive	Water	B material	B material additive	Water
	1	0.1	1.2	1	0.1	1.2

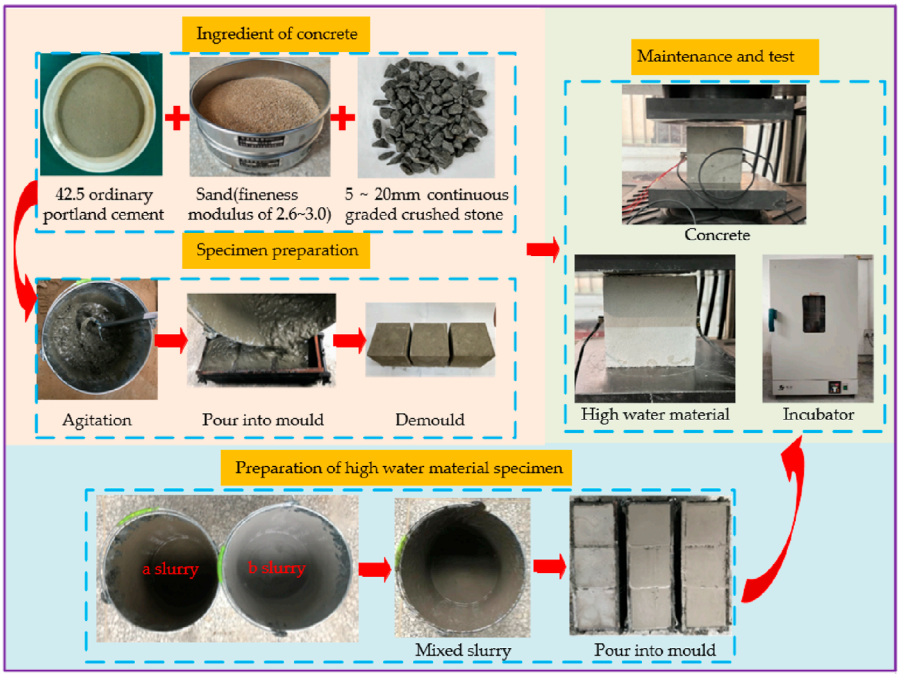

FIGURE 3
Specimen preparation and testing.

measuring 100 mm × 100 mm × 100 mm (labeled X) and high-water specimens (labeled Y) were prepared (Standard for Testing Methods of Physical and Mechanical Properties of Concrete; Zhang et al., 2024), with five specimens of each type (numbered one–5). After 3 days of curing in the incubator, the specimens were demoulded and continued to be cured in the incubator for 28 days (Zhu et al., 2017; Wang et al., 2021). The ends of the specimens were ground to a smooth finish, and the uniaxial compressive strengths of the concrete and high-water specimens were measured at 38.62 MPa and 5.91 MPa, respectively, with elastic moduli of 3.26 GPa and 0.47 GPa. The preparation and testing of the specimens are shown in Figure 3. Figure 4 presents the stress-strain curves for the concrete and high-water specimens. The experimental results suggest that the concrete specimens exhibit higher peak compressive strength and elastic modulus, with a pronounced decline in the post-peak stage of the stress-strain curve, demonstrating clear brittle characteristics. In contrast, the high-water specimens show relatively lower peak compressive strength and elastic modulus, with the post-peak stage of the stress-strain curve exhibiting distinct plastic characteristics.

2.2 Experimental equipment and experimental scheme

The preparation process for the CHWC specimens is this: ① water, cement, crushed stone, and sand were weighed according to the designed proportions. The cement, sand, and crushed stone were mixed uniformly, followed by the addition of water and thorough mixing. The resulting slurry was poured into molds (100 mm × 100 mm×100 mm) to the designed height; ② After allowing the concrete slurry to rest for 30 min, the uniformly mixed high-water slurry was filled to a height of 100 mm in the molds; ③ The specimens were placed in the incubator at a temperature of (20 ± 5)°C and a relative humidity of (95 ± 5)% (Zhu et al., 2017; Wang et al., 2021), de-molded after 3 days, and continued curing until 28 days. The composite specimens and preparation process are illustrated in Figure 5.

The uniaxial compression tests for the CHWC specimens involved five different experimental schemes, with height ratios ranging from 10% to 50%, with each experimental scheme repeated five times, experimental groups are shown in Table 2. Other height

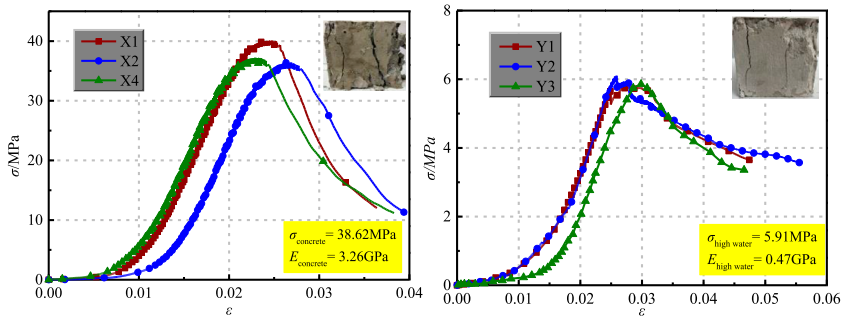

(a) (b)

FIGURE 4
Stress-strain curves of concrete and high-water materials. **(a)** Concrete. **(b)** High water materials.

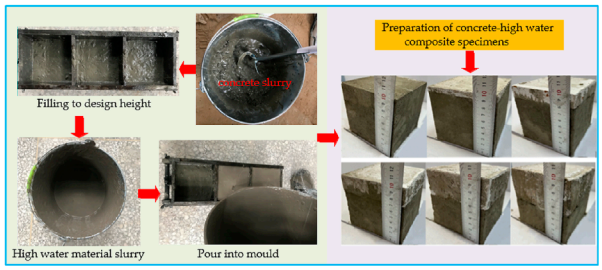

FIGURE 5
CHWC specimens and preparation process.

ratios can be further studied in subsequent experiments. The testing system comprised a loading system, a photographic system, and an AE apparatus (Figure 6). The uniaxial compression tests for the composite specimens were conducted using an MTS testing machine, with a loading rate of 0.5 MPa/min. The AE system was equipped with two RS-54A AE sensors, with a resonance frequency of 300 kHz, symmetrically positioned at the center of the left and right sides of the specimen. A preamplifier was set to 40 dB, with a threshold value of 40 dB (Zhao et al., 2013; Zhao et al., 2015 X. G.). The peak definition time (PDT), hit definition time (HDT) and hit lock time (HLT) were set to 50 μs, 100 μs, and 500 μs, respectively (Kim et al., 2015). Additionally, a hot melt gun was used as a coupling agent to attach the AE sensors to both sides of the specimen to collect AE data during loading. The AE data recorder was synchronized with the MTS testing machine to ensure data accuracy. Test environment temperature control at about 20°C.

3 Experimental results

3.1 Effect of height ratio on the stress-strain characteristic curve of CHWC specimens

Figure 7 illustrates the stress-strain relationship curve of CHWC specimens, with a typical curve shown in Figure 8. From Figures 7, 8, it can be observed that when the height ratio is 10% and 20%, the stress-strain characteristic curve can be divided into seven stages: compaction stage i, elastic stage i, plastic stage i, compaction stage ii, elastic stage ii, plastic stage ii, and failure stage, which are classified as Type I characteristic curves. The pre-peak stage of Type I curves exhibits a distinct "W" shape, demonstrating significant fluctuation characteristics, while the post-peak stage transitions from a rapid drop (PC-1) to a gradual decline (PC-2). When the height ratio ranges from 30% to 50%, the stress-strain characteristic curve of CHWC specimens generally undergoes four stages: compaction stage, elastic stage, plastic stage, and failure stage, resembling traditional stress-strain characteristic curves, thus classified as Type II characteristic curves. The post-peak of Type II curves does not exhibit a rapid drop but rather shows a trend of gradual decline, indicating notable plastic deformation characteristics. In summary, the differences between the pre-peak stages of Type I and Type II curves are significant, indicating that the height ratio has a substantial impact on the mechanical and deformation behavior of the composite specimens.

3.2 Effect of height ratio on peak compressive strength of CHWC specimens

Figure 9 presents the variation of peak compressive strength σ_c of CHWC specimens at different height ratios. Experimental data within the intermediate range were selected (excluding the maximum and minimum experimental strengths) to calculate the average peak compressive strength of the composite specimens (Ulusay, 2014), as set out in Table 3. The average value of specimen strength is calculated by eliminating the maximum and minimum values and then calculating the average of the remaining data (Ulusay, 2014). The relative deviation and relative standard deviation of the experimental results were found to be 0.69%–11.98% and 4.68%–10.37%, respectively, validating the reliability of the experimental consequences (Rohde and Feng, 1990; Kahraman, 2001). From the figures and tables, it can be deduced that as the height ratio increases from 10% to 50%, the peak compressive strength of the composite specimens decreases by 7.91 MPa (X→PC-1), 16.82 MPa (X→PC-2), 20.28 MPa (X→PC-3), 23.1 MPa (X→PC-4), and 30.93 MPa (X→PC-5), with reductions of

TABLE 2 Experimental grouping.

Specimen	Number	Percentage of concrete	Percentage of high water materials	Specimen size (mm)
Concrete	X	100%	0%	100 × 100 × 100
High water materials	Y	0%	100%	100 × 100 × 100
CHWC	PC-1	90%	10%	100 × 100 × 100
	PC-2	80%	20%	100 × 100 × 100
	PC-3	70%	30%	100 × 100 × 100
	PC-4	60%	40%	100 × 100 × 100
	PC-5	50%	50%	100 × 100 × 100

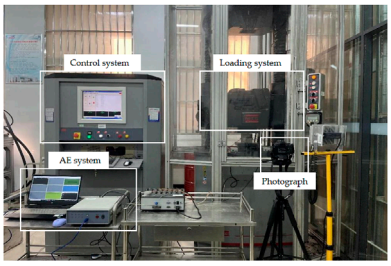

FIGURE 6
Laboratory equipment.

20.48%, 43.55%, 52.51%, 59.81%, and 80.09%, respectively. The load-bearing capacity of CHWC specimens displays a gradual decreasing trend with the increase in height ratio, yet remains higher than the peak compressive strength of high-water materials with the same mix ratio.

Zhang et al. (2024) observed that a reduced aspect ratio of specimens is associated with increased peak compressive strength. However, in this study, the peak compressive strength of CHWC specimens (38.62 MPa) is inferior to that of concrete with the same mix ratio due to uneven deformation transfer in the high-water layer during compression, which induces shear forces on the concrete's upper surface. Damage in the concrete layer during the high-water layer's deformation failure results in lower peak compressive strength for CHWC specimens compared to concrete under identical mix ratios. Conversely, CHWC specimens exhibit higher peak compressive strength than high-water materials (5.91 MPa) with the same water-cement ratio. Additionally, experimental findings reveal that increasing the proportion of high-water materials reduces the concrete layer's contribution to deformation resistance in CHWC specimens.

3.3 Effect of height ratio on elastic modulus and secant modulus of CHWC specimens

The elastic modulus E is a crucial indicator for characterizing the deformation resistance of materials. When the height ratio is between 10% and 20%, the slope of the stress-strain characteristic curve in the elastic or approximately elastic stage is selected as the elastic modulus of the composite specimen (Brady and Brown, 2013). For height proportions ranging from 30% to 50%, the slope of the curve corresponding to 40%–60% of the peak compressive stress is chosen as the elastic modulus (Cao Y. et al., 2024; Cao et al., 2025). Owing to the presence of a secondary elastic stage in the stress-strain characteristic curve of the composite specimen, relying solely on the elastic modulus is insufficient to accurately represent the mechanical properties of the composite specimen. Therefore, additional indicators such as the secant modulus S are introduced, as indicated in Table 4. The secant modulus refers to the slope of the line plugging in the origin to the point on the stress-strain curve that corresponds to 50% of the peak stress under uniaxial loading conditions. This indicator can reflect the stiffness of the specimen from either a material or structural perspective (Sun et al., 2022).

Figure 10 illustrates the variation of the secant modulus of the CHWC specimens at different height proportions. From Figure 10 and Table 4, it can be seen that the elastic modulus of the CHWC specimens fluctuates with an increasing height ratio. When the height proportion of the CHWC specimens increases from 10% to 20%, the initial elastic modulus (elastic stage i) decreases by 0.13 GPa, representing a reduction of 13.83%. The later elastic modulus (elastic stage ii) reduces by 0.54 GPa, indicating a reduction of 79.41%. Report to the elastic modulus of pure concrete specimens (3.26 GPa), the elastic modulus of CHWC specimens is significantly lower, suggesting that high-water layers enhance the ductility of CHWC specimens. Analyzing from the perspective of the secant modulus, the secant modulus of CHWC specimens generally shows a decreasing trend with the increase of high-water layers. However, at a height proportion of 40%, a significant deviation in the secant modulus is noted. Further analysis in conjunction with Section 3.1 on the stress-strain curve indicates that a height proportion of 30% is approximately the critical proportion. During loading, the CHWC specimens is on the verge of entering the compaction stage ii while the overall structure is about to fail. The fluctuation characteristics of the post-peak stage of the curve in Figure 7c can provide evidence. Therefore, from the opinion of characteristic curve I, the elastic modulus and secant modulus of CHWC specimens generally exhibit a decreasing trend (PC-1→PC-3). From the perspective

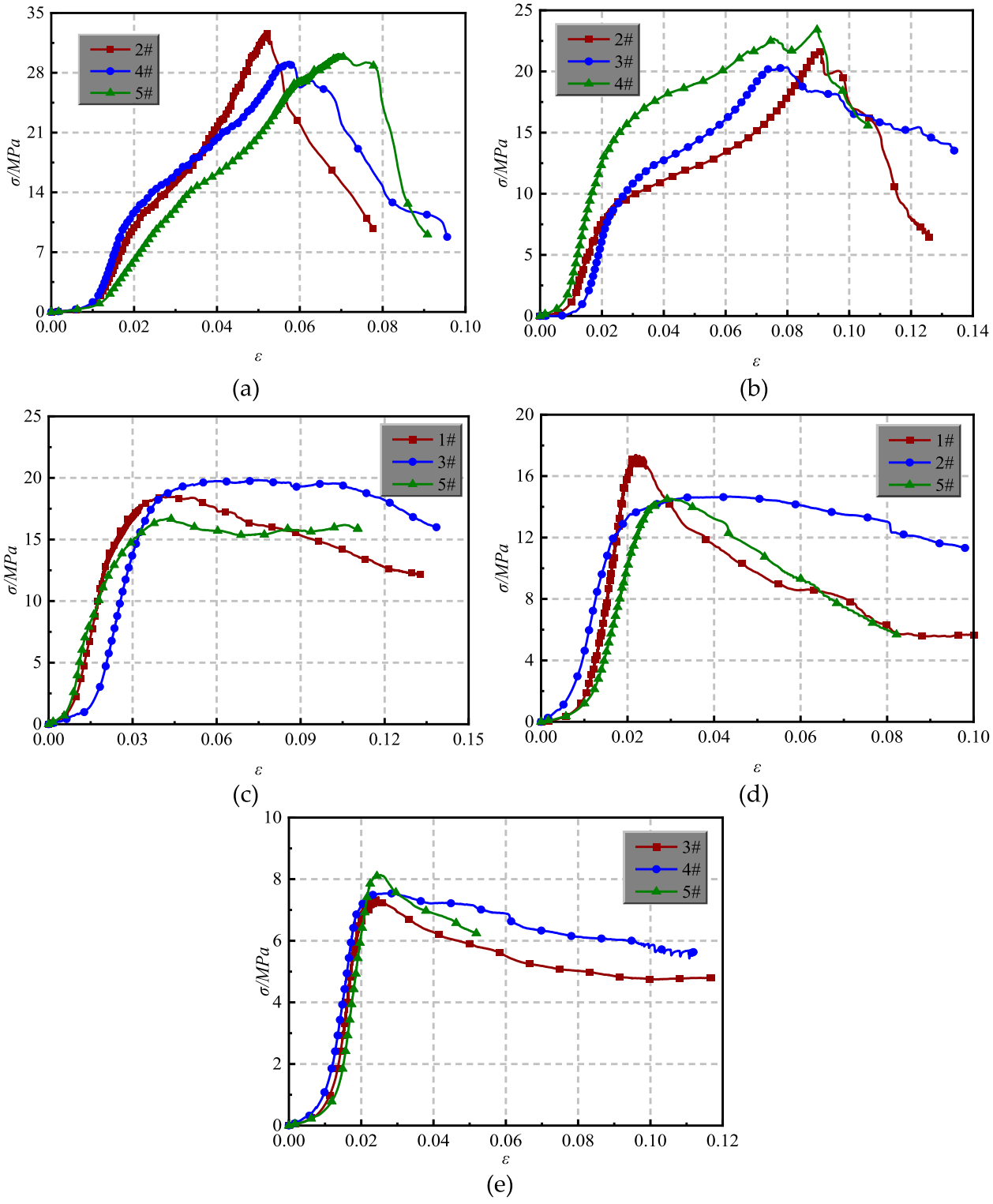

FIGURE 7
Stress-strain characteristic curves of CHWC specimens at different height ratios. **(a)** PC-1. **(b)** PC-2. **(c)** PC-3. **(d)** PC-4. **(e)** PC-5.

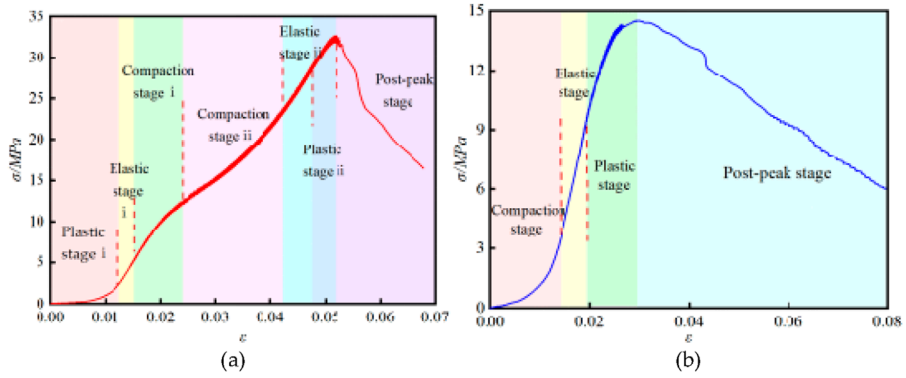

FIGURE 8
Typical stress-strain relationship curve. **(a)** Characteristic curve I. **(b)** Characteristic curve II.

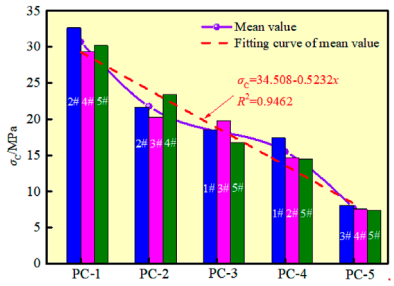

FIGURE 9
The change diagram of peak compressive strength of CHWC specimens under different height ratios. The formula *x* in the diagram refers to the height ratio.

of characteristic curves II, both the elastic modulus and secant modulus of CHWC specimens gradually decrease (PC-4→PC-5).

3.4 Effect of height ratio on peak strain of CHWC specimens

Figure 11 illustrates the peak strain variation ε_c of CHWC specimens across different height ratios, with the coefficient of variation for peak strain detailed in Table 5. The average peak strain of concrete specimens is 0.025, serving as a control group. The data indicates that peak strain in CHWC specimens initially increases and then declines with height ratios. The average peak strain variation for CHWC specimens is 124.4% (X→PC-1), 55.08% (PC-1→PC-2), attended by decreases of 38.85% (PC-2→PC-3), 44.74% (PC-3→PC-4), and 10.2% (PC-4→PC-5). At height ratios of 10% and 20%, CHWC specimens exhibit peak strains of approximately 224.4% and 348% relative to concrete specimens with the same mix ratio, demonstrating enhanced flexibility and compressive strength. At a height ratio of 30%, the coefficient of variation is 29.093%. Combined with Section 3.1, the reason for the abnormal coefficient of variation is that some curves show secondary compaction characteristics, increasing peak strain, as shown in Figure 7c (3#). At height ratios of 40% and 50%, peak strains of CHWC specimens align closely with those of concrete specimens, yet peak stress remains below 50% of that of the concrete specimens. Consequently, the load-bearing capacity and compressive performance of CHWC specimens are suboptimal. The impact of height ratio on the bearing capacity and pressure performance of the combined filling body must be thoroughly considered in the design parameters for gob-side entry retaining.

4 Macroscopic failure characteristics of CHWC specimens

Figure 12 is the macroscopic failure morphology of CHWC specimens. In the figure, the red curve represents the crack, and the shadow part represents the block spalling, summarized as follows: ① Height ratio = 10%, the high moisture layer post-failure is transformed into a thin layer due to secondary compaction, as indicated in Figure 12. Several tensile cracks are distributed across the surface of the concrete layers, penetrating from the top to the bottom of the layers, which is fundamentally similar to the failure morphology of pure concrete specimens depicted in Figure 4; ② Height ratio = 20%, the thickness of the high water layer decreases significantly, and the spalling of the bulk material is more severe. The number of penetrating cracks in the concrete layers is noticeably reduced, with a few shear cracks distributed at the edges and corners of the layer interfaces; ③ Height ratio = 30%, the concrete layers of CHWC specimens exhibit one or more tensile cracks parallel to the axial direction of the specimen, although these cracks do not penetrate through the layers. There is minor spalling of the bulk material at localized areas of the layer interface, and the post-failure high moisture layer remains relatively dense; ④ Height ratio = 40% and 50%, the high water layer experiences severe damage and significant bulk spalling. Aside from minor spalling at localized areas of the layer interface, no crack distribution is noted on the s urface, indicating that the overall structure remains relatively intact.

Based on the shape of the cracks in CHWC specimens, the initiation points of the concrete layer cracks are predominantly located at the layer interfaces. Given that the strength of the high water material is significantly lower than that of the concrete material, the high water material fails first during uniaxial loading.

TABLE 3 Peak compressive strength σ_c of CHWC specimens.

Test scenario		Peak compressive strength σ_c(MPa)	Mean value (MPa)	Absolute deviation (MPa)	Relative deviation (%)	Standard deviation (MPa)	Coefficient of variation (%)
PC-1	2#	32.64	30.71	1.93	6.28%	1.72	5.60%
	4#	29.32		1.39	4.53%		
	5#	30.18		0.53	1.73%		
PC-2	2#	21.65	21.80	0.15	0.69%	1.70	7.79%
	3#	20.32		1.48	6.79%		
	4#	23.42		1.62	7.43%		
PC-3	1#	18.48	18.34	0.14	0.76%	1.71	9.32%
	3#	19.82		1.48	8.07%		
	5#	16.71		1.63	8.89%		
PC-4	1#	17.38	15.52	1.86	11.98%	1.61	10.37%
	2#	14.67		0.85	0.05%		
	5#	14.52		1.00	6.44%		
PC-5	3#	8.10	7.69	0.41	5.33%	0.36	4.68%
	4#	7.54		0.15	1.95%		
	5#	7.43		0.26	3.38%		

As axial stress continues to be applied, the cracks penetrate the high water layer and gradually extend into the concrete layers. The concrete layers fracture under the compaction and overflow effects of the high water layer, resulting in macroscopic failure (PC-1 and PC-2) when CHWC specimens reach peak stress. However, as the height ratio continues to increase, following the failure of the high water layer, the overall load-bearing structure of CHWC specimens has already failed. The axial stress in the concrete layers does not reach its peak stress, making it difficult for penetrating cracks to appear on the surface (PC-3 and PC-4), and even leading to the absence of significant failure characteristics (PC-5).

5 Analysis of AE characteristics of CHWC specimens

For a detailed introduction regarding the quantitative characterization of crack initiation and propagation through AE, please refer to the paper (Cao et al., 2020). AE parameters and their cumulative values can be established to characterize the crack evolution features of the specimen at different stages through normalized stress curves (Eberhardt et al., 1999). Figure 13 illustrates the relationship curves of AE counts, energy, and their cumulative values with normalized stress for CHWC specimens. The cumulative value relationship curves of the characteristic parameters of CHWC specimens can be roughly classified into three stages: the AE quiet period, the low-amplitude growth period, and the high-amplitude growth period. The figure indicates that the AE counts and energy of CHWC specimens gradually decrease with an increase in height ratio. Notably, at height ratios of 40% and 50%, there is a major reduction in the cumulative values of the AE characteristic parameters. The layering of concrete did not fully utilize its load-bearing capacity during the loading failure process of CHWC specimens, which is in agreement with the findings in Sections 3.1, 3.2.

The initial growth of the cumulative value curve of AE is extremely slow, with a low slope, characterizing the AE quiet period. However, since CHWC specimens is composed of two different materials, its AE parameter characteristics differ slightly from those of a single-structure specimen, specifically manifested as follows: ① Height ratios = 10% and 20%, the cumulative value curve of the AE characteristic parameters of CHWC specimens exhibits multiple inflection points, making it difficult to determine the crack initiation threshold, as shown in Figures 12a, b. Particularly height ratio = 20%, the AE characteristic parameters of CHWC specimens show a secondary quiet period during the later loading phase. This is primarily due to secondary densification and elastic phases in CHWC specimens, resulting in very low AE signal activity and minimal energy release, which aligns with the stress-strain characteristic curves in Section 3.1; ② In the initial loading phase of some CHWC specimens, the AE ringing counts and energy are relatively high, as depicted in Figure 12c. This may be

TABLE 4 The elastic modulus *E* and secant modulus *S* of CHWC specimens under different height ratios. The number on the left side of the slash in the table is the elastic modulus of elastic stage i, and the number on the right side of the slash is the elastic modulus of elastic stage ii.

Test scenario		Elastic modulus *E* (GPa)	Mean value (GPa)	Secant modulus *S* (GPa)	Mean value (GPa)
PC-1	2#	1.15/0.93	0.94/0.68	0.51	0.48
	4#	0.96/0.65		0.51	
	5#	0.72/0.46		0.41	
PC-2	2#	0.83/0.13	0.81/0.14	0.29	0.44
	3#	0.73/0.16		0.34	
	4#	0.98/0.13		0.69	
PC-3	1#	0.43	0.40	0.31	0.27
	3#	0.40		0.21	
	5#	0.37		0.31	
PC-4	1#	1.84	1.40	0.55	0.50
	2#	1.21		0.57	
	5#	1.15		0.39	
PC-5	3#	0.77	0.79	0.24	0.24
	4#	0.67		0.26	
	5#	0.94		0.23	

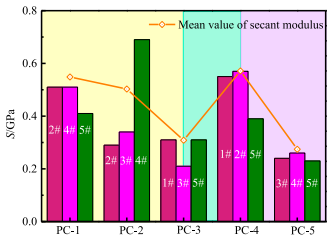

FIGURE 10
The secant modulus variation diagram of CHWC specimens under different height ratios.

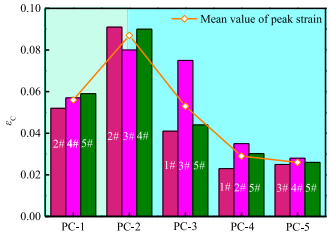

FIGURE 11
The variation curve of peak strain ε_c of CHWC specimens with height ratio.

attributed to damage occurring at the layered interface region of CHWC specimens during the early loading phase, leading to crack formation; ③ At height ratios of 30%–50%, the AE characteristic parameters and their cumulative value curves do not exhibit a secondary quiet period, and their curve characteristics are similar to those of the AE characteristic parameter curves of single-structure specimens (Liu et al., 2024; Cao et al., 2025; Cao et al., 2020).

As the external load continues to increase and reaches the crack initiation threshold of the specimen, new cracks begin to form internally, gradually propagating. This phase is characterized as the low-amplitude growth period of AE. The cumulative value curve of the AE characteristic parameters shows the first inflection point (crack initiation threshold), and it increases slowly at an approximately constant value until it reaches the second inflection point (crack damage threshold), indicating that the internal cracks of the specimen are in a stable propagation stage, as shown in Figures 13c, d. When the height ratios are 10% and 20%, the AE characteristic parameters exhibit a secondary low-amplitude growth period. In the later loading phase of CHWC specimens, the slope of the cumulative value curve of AE decreases, indicating that the extent of crack propagation during this stage is less than in the earlier phase. Under the continuous action of external loads, as CHWC specimens gradually reaches the crack damage threshold, cracks begin to connect and propagate to the surface of the specimen, accompanied by a significant generation of AE signals and the release of substantial energy. This stage is

TABLE 5 Peak strain ε_c of CHWC specimens.

Test case		Peak strain ε_c	Mean value	Absolute Deviation	Relative Deviation (%)	Standard Deviation	Coefficient of variation (%)
PC-1	2#	0.0519	0.0561	0.0042	7.487	0.0030	5.420
	4#	0.0574		0.0013	2.317		
	5#	0.0590		0.0029	5.169		
PC-2	2#	0.0910	0.0870	0.0040	4.598	0.0050	5.709
	3#	0.0800		0.0070	8.046		
	4#	0.0900		0.0030	3.448		
PC-3	1#	0.0406	0.0532	0.0126	23.684	0.0155	29.093
	3#	0.0750		0.0218	40.977		
	5#	0.0440		0.0092	17.293		
PC-4	1#	0.0230	0.0294	0.0064	21.769	0.0049	16.667
	2#	0.0350		0.0056	19.048		
	5#	0.0302		0.0008	2.721		
PC-5	3#	0.0250	0.0264	0.0014	5.422	0.0014	5.227
	4#	0.0283		0.0019	7.062		
	5#	0.0260		0.0004	1.639		

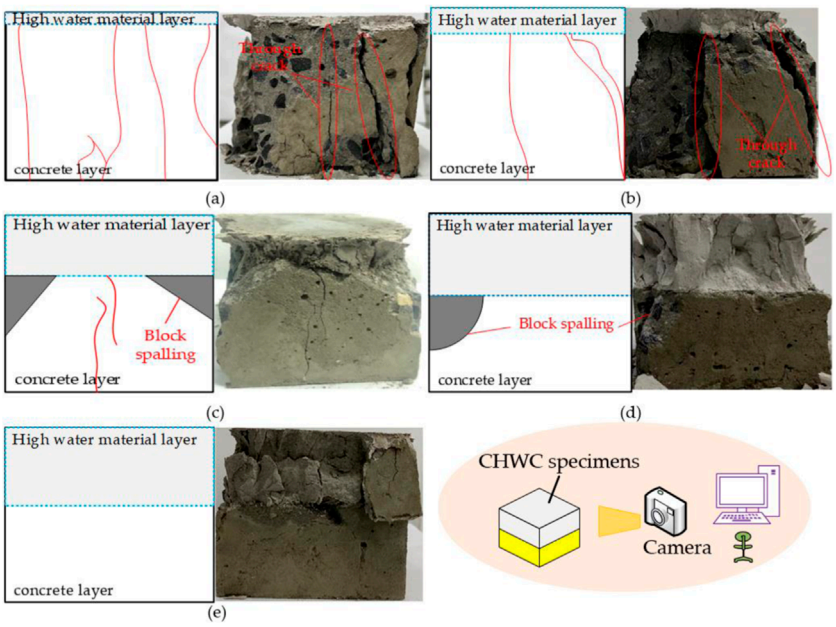

FIGURE 12
Macroscopic failure morphology of CHWC specimens with different height ratios. **(a)** PC-1. **(b)** PC-2. **(c)** PC-3. **(d)** PC-4. **(e)** PC-5.

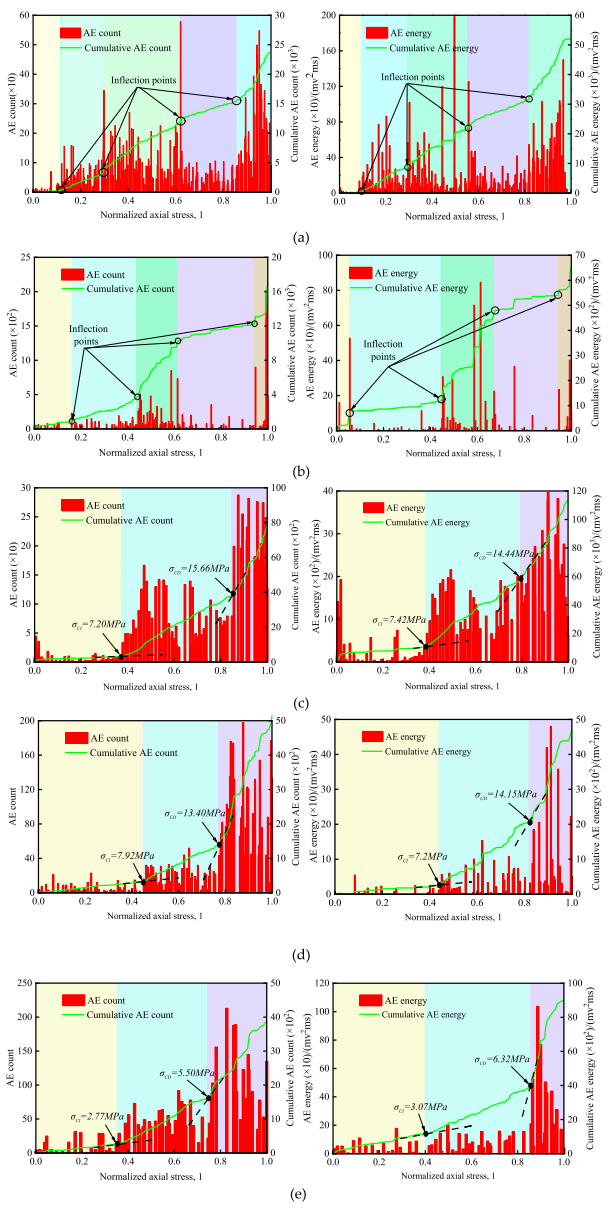

FIGURE 13
Relationship curves of "AE properties (count and energy) and cumulative values normalized to stress" for CHWC specimens at different height ratio. **(a)** PC-1. **(b)** PC-2. **(c)** PC-3. **(d)** PC-4. **(e)** PC-5.

characterized as the high-amplitude growth period of AE. At height ratios of 10% and 20%, the high water layers deform and fail during the early stress loading phase, leading to the emergence of the high-amplitude growth period in the mid-range of the cumulative value curve, while this feature is absent at height ratios of 30%–50%.

6 Discussion

The mechanical behavior of CHWC specimens is not only closely related to the strength of the filling material, material properties, and loading methods (Karacan, 2015; Cao et al., 2019; Yu et al., 2021). It is also influenced by the height ratio and the characteristics of the layered interfaces (Lei et al., 2023; Bingchao et al., 2023). The height ratio of the layers is one of the critical factors affecting the mechanical performance of CHWC specimens (Liu et al., 2019). As the height ratio increases, the peak compressive strength of CHWC specimens gradually decreases, while the peak strain initially increases and then decreases. During the early stages of loading, the concrete layers, high water layers, and layered interfaces are all compacted. As the axial stress increases, the concrete layers and high water layers undergo axial deformation. Given that the strength and elastic modulus of concrete are significantly greater than those of the high water material, micro-cracks within the high water layer gradually develop and propagate. The cracks interconnect, forming through-cracks, leading to the failure of the high water layer before that of the concrete layers. Analyzing the stress-strain curves and AE characteristics, the specimens exhibit a plastic phase in the early loading stage, accompanied by a significant number of AE events, as illustrated in Figures 7a, b and Figures 12a, b. Due to the "interface effect" of CHWC specimens, the lateral deformation of concrete is enhanced during the failure process of high water materials. The interlayer friction reduces the CI threshold of the concrete, causing it to crack under relatively low axial stress. Even when the aspect ratio of CHWC specimen is less than that of pure concrete specimens, the peak compressive strength of CHWC specimens remains lower than that of pure concrete specimens. When the proportion of high water materials is significant, the mechanical properties of CHWC specimens are dominated by the high water materials. As the aspect ratio of the high water materials increases, the peak compressive strength of CHWC specimens gradually decreases. Cao et al. (2019) and Bingchao et al. (2023) noted that the peak strength of composite specimens is negatively correlated with the height of weak layers and positively correlated with the height of strong layers, which is consistent with the findings of this study.

The failure mode of CHWC specimens is also influenced by the height ratio. When the height ratio is between 10% and 20%, under sustained stress, the high water layer that fails is gradually compacted and transmits stress to the concrete layers. Cracks within the concrete layer gradually develop and interconnect, forming tensile cracks that penetrate through the top and bottom of the layers. Analyzing the failure morphology of pure concrete and high water specimens, within this height ratio range, CHWC specimens primarily exhibit tensile failure. The concrete layers play a dominant role in the compressive failure of CHWC specimens. When the height ratio is between 30% and 40%, the failure mode of the high water layer at this stage involves the spalling of edge blocks and particle sliding due to the failure of the internal cement matrix. The spalling and sliding of local blocks lead to non-uniform deformation at the layered interfaces (Liu et al., 2024). As the axial stress further increases, shear stress develops at the layered interfaces of CHWC specimens, causing stress concentration phenomena (Bingchao et al., 2023), ultimately resulting in localized shear failure at the edges of the concrete layers, as shown in Figures 12c, d. When the height ratio reaches 50%, the stress at which the overall structure of CHWC specimens fails is insufficient to cause shear failure of the concrete layers. As the height ratio increases, observable cracks and spalling phenomena on the surface of the concrete layers gradually disappear, while the peak compressive strength of CHWC specimens decreases. The results of this study can be used

as a reference for the application of combined filling technology in gob-side entry retaining. However, it is worth noting that the above experimental results are limited to the mechanical behavior of CHWC specimens under uniaxial compression. When the layered materials, layer strengths, and external loading methods of the specimens change, the research findings will need to be revised accordingly.

7 Conclusion

This study aims to investigate the influence of height ratio on the mechanical properties of CHWC specimens, with the main conclusions as follows.

(1) The peak compressive strength of CHWC specimens exhibits a negative correlation with the proportion of high-water layers and a positive correlation with the proportion of concrete layers. When the height ratio is 10% and 20%, the mechanical properties of CHWC specimens are dominated by concrete. However, at height ratio of 30%–50%, the mechanical properties of CHWC specimens are primarily governed by the high-water materials.

(2) The peak strain of CHWC specimens initially increases and then decreases with the increase in height ratio. As the height ratio increases from 10% to 50%, the peak strains of CHWC specimens are 224.4%, 348%, 212.8%, 117.6%, and 105.6% of the peak strain of the concrete samples with the same mix ratio, respectively.

(3) When the height ratio is between 10% and 20%, CHWC specimens predominantly fail in tension, with the high-water materials exerting a significant tearing effect on the concrete. In contrast, at height ratio of 30%–50%, the high-water layers primarily fail in tension, while the concrete layers predominantly experience localized shear failure. Following the failure of the high-water layers, the overall load-bearing structure of CHWC specimens becomes compromised.

Data availability statement

The original contributions presented in the study are included in the article/supplementary material, further inquiries can be directed to the corresponding authors.

Author contributions

YC: Funding acquisition, Writing – original draft. LS: Writing – review and editing. XZ: Writing – review and editing. ZX: Writing – review and editing. LT: Writing – review and editing. YZ: Writing – review and editing. PW: Writing – review and editing.

Funding

The author(s) declare that financial support was received for the research and/or publication of this article. This work was supported by the National Natural Science Foundation of China for Young (No.52404147, No.52304102), Youth Science and Technology Fund of China University of Mining and Technology (No.2024QN11079).

Conflict of interest

The authors declare that the research was conducted in the absence of any commercial or financial relationships that could be construed as a potential conflict of interest.

Generative AI statement

The author(s) declare that no Generative AI was used in the creation of this manuscript.

Publisher's note

All claims expressed in this article are solely those of the authors and do not necessarily represent those of their affiliated organizations, or those of the publisher, the editors and the reviewers. Any product that may be evaluated in this article, or claim that may be made by its manufacturer, is not guaranteed or endorsed by the publisher.

References

Bingchao, Z., Jingbin, W., Qing, Z., Yunxiang, M. A., Di, Z., Pan, C., et al. (2023). Experimental study on mechanical properties of filling-bulk ce-menting combination body. *mtkxjs* 51, 298–309. doi:10.13199/j.cnki.cst.2022-0911

Brady, B., and Brown, E. (2013). *Rock mechanics: for underground mining*. Berlin: Springer.

Cao, S., Xue, G., and Song, W. (2019). Experimental research on mechanical properties of combined cemented tailings backfill and its application. *J. Min. Saf. Eng.* 36, 601–608. doi:10.13545/j.cnki.jmse.2019.03.022

Cao, X., Wang, S., Wang, X., Lei, P., and chen, W. (2024a). Non-pillar mining of upper coal seam layers with double-roadway driving using a flexible-formwork pre-cast partition wall. *Meas. Sci. Technol.* 35, 105601. doi:10.1088/1361-6501/ad6027

Cao, Y., Xu, J., Chen, L., Wu, P., and Shaikh, F. (2020). Experimental study on granite acoustic emission and micro-fracture behavior with combined compression and shear loading: phenomenon and mechanism. *Sci. Rep.* 10, 22051. doi:10.1038/s41598-020-78137-0

Cao, Y., Xu, Z., Tai, L., Kong, Z., Wu, P., Li, C., et al. (2024b). Experimental study on the mechanical properties and damage mechanism of saturated coal-measure sandstone in an open pit mine under the freeze–thaw effect. *Appl. Sci.* 14, 11381. doi:10.3390/app142311381

Cao, Y., Zhang, X., Sun, L., Zheng, Y., and Li, C. (2025). Mechanical properties and macro–micro failure mechanisms of granite under thermal treatment and inclination. *Geomech. Geophys. Geo-energ. Geo-resour.* 11, 8. doi:10.1007/s40948-024-00925-z

Chen, D., Wang, X., Wu, S., Zhang, F., Fan, Z., Wang, X., et al. (2023). Study on stability mechanism and control techniques of surrounding rock in gob-side entry retaining with flexible formwork concrete wall. *J. Cent. South Univ.* 30, 2966–2982. doi:10.1007/s11771-023-5436-z

Chen, M., Wang, H., Qi, M., Li, Y., Wang, S., and Wang, E. (2020). Experimental study on dynamic compressive properties of composite layers of rock and steel fiber reinforced concrete. *Chin. J. Rock Mech. Eng.* 39, 1222–1230. doi:10.13722/j.cnki.jrme.2019.1221

Cheng, Z., Li, L.-H., and Zhang, Y.-N. (2020). Laboratory investigation of the mechanical properties of coal-rock combined body. *Bull. Eng. Geol. Environ.* 79, 1947–1958. doi:10.1007/s10064-019-01613-z

Eberhardt, E., Stead, D., and Stimpson, B. (1999). Quantifying progressive pre-peak brittle fracture damage in rock during uniaxial compression. *Int. J. Rock Mech. Min. Sci.* 36, 361–380. doi:10.1016/S0148-9062(99)00019-4

Guo, D., Zuo, J., Zhang, Y., and Yang, R. (2011). Research on strength and failure mechanism of deep coal-rock combination bodies of different inclined angles. *Rock Soil Mech.* 32, 1333–1339. doi:10.16285/j.rsm.2011.05.029

He, Y., Zhao, P., Li, S., Ho, C.-H., Zhu, S., Kong, X., et al. (2021). Mechanical properties and energy dissipation characteristics of coal–rock-like composite materials subjected to different rock–coal strength ratios. *Nat. Resour. Res.* 30, 2179–2193. doi:10.1007/s11053-021-09850-4

Jianbiao, B. a. I., Zizheng, Z., Xiangyu, W., Ying, X. U., Shuai, Y. a. N., and Jun, X. U. (2022). Stress control and surrounding rock strengthening mechanism of gob-side entry retaining with high-water content material filling and its application. *mtkxjs* 50, 16–28. doi:10.13199/j.cnki.cst.2022-0257

Kahraman, S. (2001). Evaluation of simple methods for assessing the uniaxial compressive strength of rock. *Int. J. Rock Mech. Min. Sci.* 38, 981–994. doi:10.1016/S1365-1609(01)00039-9

Karacan, C. Ö. (2015). Analysis of gob gas venthole production performances for strata gas control in longwall mining. *Int. J. Rock Mech. Min. Sci.* 79, 9–18. doi:10.1016/j.ijrmms.2015.08.001

Kim, J.-S., Lee, K.-S., Cho, W.-J., Choi, H.-J., and Cho, G.-C. (2015). A comparative evaluation of stress–strain and acoustic emission methods for quantitative damage assessments of brittle rock. *Rock Mech. Rock Eng.* 48, 495–508. doi:10.1007/s00603-014-0590-0

Kong, D., Pu, S., Cheng, Z., Wu, G., and Liu, Y. (2021). Coordinated deformation mechanism of the top coal and filling body of gob-side entry retaining in a fully mechanized caving face. *Int. J. Geomechanics* 21, 04021030. doi:10.1061/(ASCE)GM.1943-5622.0001972

Koupouli, N., Tikou, B., and Effenguet, H. (2016). Direct shear tests on cemented paste backfill-rock wall and cemented paste backfill-backfill interfaces. *J. Rock Mech. Geotechnical Eng.* 8, 472–479. doi:10.1016/j.jrmge.2016.02.001

Lei, S., Hao, D., and Cao, S. (2023). Study on uniaxial compression deformation and fracture development characteristics of weak interlayer coal–rock combination. *Fractal Fract.* 7, 731. doi:10.3390/fractalfract7100731

Li, G., Wang, H., Liu, Z., Liu, H., Yan, H., and Liu, Z. (2023). Effects of aeolian sand and Water–Cement ratio on performance of a novel mine backfill material. *Sustainability* 15, 569. doi:10.3390/su15010569

Li, X., and Liu, C. (2018). Mechanical properties and damage constitutive model of high water material at different loading rates. *Adv. Eng. Mater.* 20, 1701098. doi:10.1002/adem.201701098

Liu, H., Liu, C., Yue, X., and Wang, J. (2024). Study on mechanical properties and acoustic emission characteristics of mudstone-clay composites under uniaxial compression. *Eng. Geol.* 332, 107478. doi:10.1016/j.enggeo.2024.107478

Liu, W., Yuan, W., Yan, Y., and Wang, X. (2019). Analysis of acoustic emission characteristics and damage constitutive model of coal-rock combined body based on particle flow code. *Symmetry* 11, 1040. doi:10.3390/sym11081040

Lu, J., Huang, G., Gao, H., Li, X., Zhang, D., and Yin, G. (2020). Mechanical properties of layered composite coal–rock subjected to true triaxial stress. *Rock Mech. Rock Eng.* 53, 4117–4138. doi:10.1007/s00603-020-02148-6

Ma, B., Wang, F., Liu, H., Yin, D., and Xia, Z. (2022). Mechanical properties of rock–coal–rock composites at different inclined coal seam thicknesses. *Front. Phys.* 9. doi:10.3389/fphy.2021.806055

Ma, Q., Tan, Y., Liu, X., Zhao, Z., and Fan, D. (2021). Mechanical and energy characteristics of coal–rock composite sample with different height ratios: a numerical study based on particle flow code. *Environ. Earth Sci.* 80, 309. doi:10.1007/s12665-021-09453-5

Pan, B., Yu, W., and Shen, W. (2021). Experimental study on energy evolution and failure characteristics of rock–coal–rock combination with different height ratios. *Geotech. Geol. Eng.* 39, 425–435. doi:10.1007/s10706-020-01501-4

Rohde, J., and Feng, H. (1990). Analysis of the variability of unconfined compression tests of rock. *Rock Mech. Rock Engng* 23, 231–236. doi:10.1007/BF01022955

Selçuk, L., and Aşma, D. (2019). Experimental investigation of the Rock–Concrete bi materials influence of inclined interface on strength and failure behavior. *Int. J. Rock Mech. Min. Sci.* 123, 104119. doi:10.1016/j.ijrmms.2019.104119

Sun, M., Hu, G., Hu, J., Zhang, H., Li, Y., Wang, W., et al. (2022). Simulation study on the size effect of secant modulus of rocks containing rough joints. *Sustainability* 14, 15640. doi:10.3390/su142315640

Tan, Y., Yu, X., Song, W., Wang, H., and Cao, S. (2018). Experimental study on combined pressure-bearing mechanism of filling body and surrounding rock. *Caikuang yu Anquan Gongcheng Xuebao/Journal Min. Saf. Eng.* 35, 1071–1076. doi:10.13545/j.cnki.jmse.2018.05.026

Tian, Z., Zhang, Z., Deng, M., Yan, S., and Bai, J. (2020). Gob-side entry retained with soft roof, floor, and seam in thin coal seams: a case study. *Sustainability* 12, 1197. doi:10.3390/su12031197

Ulusay, R. (2014). *The ISRM suggested methods for rock characterization, testing and monitoring: 2007-2014*. New York: Springer.

Wang, J., Jiang, F., Meng, X., Wang, X., Zhu, S., and Feng, Y. (2016). Mechanism of rock burst occurrence in specially thick coal seam with rock parting. *Rock Mech. Rock Eng.* 49, 1953–1965. doi:10.1007/s00603-015-0894-8

Wang, K., Zhao, E., Guo, Y., Du, F., and Ding, K. (2024). Effect of loading rate on the mechanical and seepage characteristics of gas-bearing coal–rock and its mechanical constitutive model. *Phys. Fluids* 36, 026606. doi:10.1063/5.0192035

Wang, X., Xie, J., Xu, J., Zhu, W., and Wang, L. (2021). Effects of coal mining height and width on overburden subsidence in longwall pier-column backfilling. *Appl. Sci.* 11, 3105. doi:10.3390/app11073105

Wu, G., Yu, W., Zuo, J., and Du, S. (2020). Experimental and theoretical investigation on mechanisms performance of the rock-coal-bolt (RCB) composite system. *Int. J. Min. Sci. Technol.* 30, 759–768. doi:10.1016/j.ijmst.2020.08.002

Wu, J., Jing, H., Gao, Y., Meng, Q., Yin, Q., and Du, Y. (2022). Effects of carbon nanotube dosage and aggregate size distribution on mechanical property and microstructure of cemented rockfill. *Cem. Concr. Compos.* 127, 104408. doi:10.1016/j.cemconcomp.2022.104408

Wu, J., Wong, H. S., Zhang, H., Yin, Q., Jing, H., and Ma, D. (2024). Improvement of cemented rockfill by premixing low-alkalinity activator and fly ash for recycling gangue and partially replacing cement. *Cem. Concr. Compos.* 145, 105345. doi:10.1016/j.cemconcomp.2023.105345

Wu, J., Yang, S., Williamson, M., Wong, H. S., Bhudia, T., Pu, H., et al. (2025a). Microscopic mechanism of cellulose nanofibers modified cemented gangue backfill materials. *Adv. Compos Hybrid. Mater* 8, 177. doi:10.1007/s42114-025-01270-9

Wu, J., Yang, S., Wong, H. S., Yin, Q., Zhang, H., Chen, W., et al. (2025b). Reinforcement mechanisms of cellulose nanofibers on cemented rockfill: macroscopic, microscopic and molecular insights. *Constr. Build. Mater.* 466, 140192. doi:10.1016/j.conbuildmat.2025.140192

Wu, P., Wang, Y., Chiu, Y., Li, Y., and Lin, T.-Y. (2019). Production efficiency and geographical location of Chinese coal enterprises - undesirable EBM DEA. *Resour. Policy* 64, 101527. doi:10.1016/j.resourpol.2019.101527

Yin, D., Chen, S., Jiang, N., and Sun, X. (2019). Strength characteristics of roof rock-coal composite samples with different height ratios under uniaxial loading. *Archives Min. Sci.* 64, 307–319. doi:10.24425/AMS.2019.128685

Yu, W., Wu, G., Pan, B., Wu, Q., and Liao, Z. (2021). Experimental investigation of the mechanical properties of sandstone–coal–bolt specimens with different angles under conventional triaxial compression. *Int. J. Geomechanics* 21, 04021067. doi:10.1061/(ASCE)GM.1943-5622.0002005

Zhang, J., Zhou, Y., Xiao, Y., Wang, M., Liu, S., Yang, Z., et al. (2023). A study on the characteristics of high-solid-water filling materials with different water contents based on the Boltzmann superposition principle. *Sustainability* 15, 9675. doi:10.3390/su15129675

Zhang, W., Yan, C., Zhou, G., Guo, J., Chen, Y., Zhang, B., et al. (2022). Experimental and analytical investigation into the synergistic mechanism and failure characteristics of the backfill-red sandstone combination. *Minerals* 12, 202. doi:10.3390/min12020202

Zhang, X., Yao, W., Wang, X., Li, W., Zhu, X., and Huang, H. (2024). Experimental study on mechanical properties of low-strength mortar–granite composite specimens. *Rock Mech. Rock Eng.* 57, 11083–11098. doi:10.1007/s00603-024-04129-5

Zhao, K., Huang, M., Zhou, Y., Yan, Y., Wan, W., Ning, F., et al. (2022). Synergistic deformation in a combination of cemented paste backfill and rocks. *Constr. Build. Mater.* 317, 125943. doi:10.1016/j.conbuildmat.2021.125943

Zhao, X. G., Cai, M., Wang, J., Li, P. F., and Ma, L. K. (2015a). Objective determination of crack initiation stress of brittle rocks under compression using AE measurement. *Rock Mech. Rock Eng.* 48, 2473–2484. doi:10.1007/s00603-014-0703-9

Zhao, X. G., Cai, M., Wang, J., and Ma, L. K. (2013). Damage stress and acoustic emission characteristics of the Beishan granite. *Int. J. Rock Mech. Min. Sci.* 64, 258–269. doi:10.1016/j.ijrmms.2013.09.003

Zhao, Z., Wang, W., Wang, L., and Dai, C. (2015b). Compression–shear strength criterion of coal–rock combination model considering interface effect. *Tunn. Undergr. Space Technol.* 47, 193–199. doi:10.1016/j.tust.2015.01.007

Zhu, W., Xu, J., Xu, J., Chen, D., and Shi, J. (2017). Pier-column backfill mining technology for controlling surface subsidence. *Int. J. Rock Mech. Min. Sci.* 96, 58–65. doi:10.1016/j.ijrmms.2017.04.014

Zhu, Y., Tian, Y., Gong, P., Wen, G., and Yi, K. (2024). Predictive model for the instability of flexible formwork concrete wall in secondary mining of non-pillar coal mining. *Sci. Rep.* 14, 21684. doi:10.1038/s41598-024-72883-1